






## Article

# Microstructure and Properties of TiB<sub>2</sub> Composites Produced by Spark Plasma Sintering with the Addition of Ti<sub>5</sub>Si<sub>3</sub>

Agnieszka Twardowska <sup>1,\*</sup>, Marcin Podsiadło <sup>2</sup>, Iwona Sulima <sup>1</sup>, Krzysztof Bryła <sup>1</sup> and Paweł Hyjek <sup>1</sup>

<sup>1</sup> Institute of Technology, Pedagogical University, 2 Podchorążych, 30-084 Krakow, Poland; iwona.sulima@up.krakow.pl (I.S.); krzysztof.bryla@up.krakow.pl (K.B.); pawel.hyjek@up.krakow.pl (P.H.)

<sup>2</sup> Łukasiewicz Research Network–Krakow Institute of Technology, 73 Zakopianska, 30-418 Krakow, Poland; marcin.podsiadlo@kit.lukasiewicz.gov.pl

\* Correspondence: agnieszka.twardowska@up.krakow.pl

**Abstract:** Titanium diboride (TiB<sub>2</sub>) is a hard, refractory material, attractive for a number of applications, including wear-resistant machine parts and tools, but it is difficult to densify. The spark plasma sintering (SPS) method allows producing TiB<sub>2</sub>-based composites of high density with different sintering aids, among them titanium silicides. In this paper, Ti<sub>5</sub>Si<sub>3</sub> is used as a sintering aid for the sintering of TiB<sub>2</sub>/10 wt % Ti<sub>5</sub>Si<sub>3</sub> and TiB<sub>2</sub>/20 wt % Ti<sub>5</sub>Si<sub>3</sub> composites at 1600 °C and 1700 °C for 10 min. The phase composition of the initial powders and produced composites was analyzed by the X-ray diffraction method using CuK<sub>α</sub> radiation. The microstructure was examined using scanning electron microscopy, accompanied by energy-dispersive spectroscopy (EDS). The hardness was determined using a diamond indenter of Vickers geometry loaded at 9.81 N. Friction–wear properties were tested in the dry sliding test in a ball-on-disc configuration, using WC as a counterpart material. The major phases present in the TiB<sub>2</sub>/Ti<sub>5</sub>Si<sub>3</sub> composites were TiB<sub>2</sub> and Ti<sub>5</sub>Si<sub>3</sub>. Traces of TiC were also identified. The hardness of the TiB<sub>2</sub>/Ti<sub>5</sub>Si<sub>3</sub> composites was in the range of 1860–2056 HV<sub>1</sub> and decreased with Ti<sub>5</sub>Si<sub>3</sub> content, as well as the specific wear rate W<sub>v</sub>. The coefficient of friction for the composites was in the range of 0.5–0.54, almost the same as for TiB<sub>2</sub> sinters. The main mechanism of wear was abrasive.

**Keywords:** TiB<sub>2</sub>; Ti<sub>5</sub>Si<sub>3</sub>; spark plasma sintering; hardness; friction–wear properties



**Citation:** Twardowska, A.; Podsiadło, M.; Sulima, I.; Bryła, K.; Hyjek, P. Microstructure and Properties of TiB<sub>2</sub> Composites Produced by Spark Plasma Sintering with the Addition of Ti<sub>5</sub>Si<sub>3</sub>. *Materials* **2021**, *14*, 3812. <https://doi.org/10.3390/ma14143812>

Academic Editor: Miguel Alguero

Received: 31 May 2021

Accepted: 5 July 2021

Published: 8 July 2021

**Publisher's Note:** MDPI stays neutral with regard to jurisdictional claims in published maps and institutional affiliations.



**Copyright:** © 2021 by the authors. Licensee MDPI, Basel, Switzerland. This article is an open access article distributed under the terms and conditions of the Creative Commons Attribution (CC BY) license (<https://creativecommons.org/licenses/by/4.0/>).

## 1. Introduction

The most extensively studied phase in the Ti-B system is titanium diboride, as it is the hardest and most thermodynamically stable. It is characterized by an extremely high melting point (3225 °C), high hardness (35–40 GPa) and Young's modulus (450 GPa), which are associated with relatively high thermal (60–120 W/mK) and electrical conductivities (~10<sup>5</sup> S/cm) [1]. Due to this unique set of properties, titanium diboride is an attractive material for a number of applications, including cutting tools, wear-resistant parts and coatings, ballistic armor, cathodes in Hall–Heroult cells for aluminum smelting, crucibles for handling molten metals and metal evaporation boats [1,2]. TiB<sub>2</sub> crystallizes in a hexagonal closely packed crystal lattice (P6/mmm space group) with elementary unit cell parameters of a = 3.02 Å and c = 3.22 Å. The anisotropy of its thermal expansion coefficient is believed to be a source of microcrack formation and brittleness, observed either at the synthesis stage of TiB<sub>2</sub> or thermal cycles taking place afterward both in bulk materials and thin films [3]. A low self-diffusion coefficient and an extremely high melting point make it difficult to obtain TiB<sub>2</sub> sinters of high density [4,5]. Among the different sintering methods, the most effective and fastest is spark plasma sintering (SPS). It was demonstrated that by the SPS method, using simultaneously pulsed direct current and uniaxial pressure, TiB<sub>2</sub> sinters of 96% theoretical density could be produced within 10 min at a temperature range of 1200–1800 °C, but the produced sinters were susceptible to cracking. To limit the brittleness of TiB<sub>2</sub> sinters, sintering aids have been introduced. The use of sintering additives is

advantageous for the density and temperature of sintering. Metal additives are effective in lowering the sintering temperature, but at the cost of lowering the mechanical properties. Among the ceramic aids used for TiB<sub>2</sub> sintering are TiC [6], MoSi<sub>2</sub> [7] and TiSi<sub>2</sub> [8,9]. It was demonstrated that TiB<sub>2</sub>/TiSi<sub>2</sub> composites with a TiSi<sub>2</sub> content of 5–15 wt % produced by SPS at a temperature range of 1200–1400 °C can achieve high density (~98% of the theoretical density) [9]. It was found that the addition of TiSi<sub>2</sub> enhances the densification, lowers the temperature of sintering and is beneficial for the mechanical properties of TiB<sub>2</sub>-based composites; however, due to the melting point of TiSi<sub>2</sub>, which is 1464 °C, the working temperature of the produced composites is limited. There are four titanium silicides in the Ti-Si system, among them Ti<sub>5</sub>Si<sub>3</sub> (Mn<sub>5</sub>Si<sub>3</sub> crystal structure type), which is the most thermodynamically stable [10]. In comparison to TiSi<sub>2</sub>, Ti<sub>5</sub>Si<sub>3</sub> is characterized by a lower density (4.32 g/cm<sup>3</sup>), a higher melting point (2130 °C), higher hardness and resistance to oxidation, so it is also an attractive material to be used as a sintering aid for TiB<sub>2</sub>-based composites [8]. Research on the use of this titanium silicide as a sintering additive is scarce because of its brittleness, which may adversely affect the properties of the obtained composites. Therefore, most studies concern the content of this silicide up to 5%. The aim of this study is to densify TiB<sub>2</sub>/Ti<sub>5</sub>Si<sub>3</sub> micropowders by the SPS method and to study the influence of Ti<sub>5</sub>Si<sub>3</sub> addition on the microstructure, hardness and friction–wear properties of the produced composites.

## 2. Materials and Methods

### 2.1. Powders, Powder Mixtures and Parameters of Their Homogenization

Two commercially available powders were used: TiB<sub>2</sub> (Sigma-Aldrich, Darmstadt Germany) of 99.9 wt % chemical purity, grain size = <10 µm, density = 4.52 g/cm<sup>3</sup>; Ti<sub>5</sub>Si<sub>3</sub> (Alfa Aesar, Kandel, Germany) of 99.5 wt % chemical purity, grain size = <10 µm, density = 4.32 g/cm<sup>3</sup>. Two powder mixtures were investigated: TiB<sub>2</sub> + 10 wt % Ti<sub>5</sub>Si<sub>3</sub> and TiB<sub>2</sub> + 20 wt. % Ti<sub>5</sub>Si<sub>3</sub>. The powder mixtures were homogenized three times in SpeedMixer TM DAC 400.1 FVZ (Hauschild & Co. KG, Hamm, Germany) at a rotational speed of 2000 RPM and a rotation time of 30 s, followed by a 10 s break.

### 2.2. Spark Plasma Sintering

Spark plasma sintering was conducted using FCT Systeme GmbH (Effelder-Rauenstein, Germany), model HP D 5, and graphite die with an inner diameter of 20 mm. Densification of powders started with initial degassing by pressing for 10 min in vacuum ( $5 \times 10^{-1}$  mbar) to the maximum pressure of 35 MPa. After that, the furnace chamber was filled with argon, heated up at a rate of 200 °C/min to the selected sintering temperature (1600 °C and 1700 °C), held for 10 min then cooled down at a rate of 200 °C/min.

### 2.3. Relative Density, Microstructure Examination

Sintered samples were mechanically ground and polished on one side using diamond grinding (9, 6 and 3 µm) and polishing suspensions (1 µm), respectively. At each grinding step, samples were degreased in isopropanol, ultrasonically cleaned in distilled water for 5 min and dried in air. The relative densities of the composites were determined by the Archimedes immersion method by measuring the weight differences of the specimens in air and in ethanol pure at room-temperature conditions. The theoretical densities of the samples were calculated according to the rule of mixtures. Phase compositions of powders and sinters were analyzed by the X-ray diffraction method (XRD) in Bragg–Brentano geometry using CuK $\alpha$  radiation ( $\lambda = 1.5406 \text{ \AA}$ ,  $U = 40 \text{ kV}$ ,  $I = 30 \text{ mA}$ ). The XRD patterns were collected in 2 $\theta$  geometry over scattering angles ranging from 20° to 90° with a step size of 0.02°. Phase identification was performed according to The International Centre for Diffraction Data (ICDD<sup>®</sup>) database. The microstructure of the samples was observed by the scanning electron microscope (SEM) JEOL JSM-6610 LV (JEOL Ltd., Tokyo, Japan) with energy-dispersive X-ray spectroscopy (EDS) using the X-Max detector (Oxford Instruments, Abingdon, UK), equipped with Aztec 2.1 software.

#### 2.4. Hardness and Friction–Wear Tests

Hardness was determined using the NEXUS 4000 hardness tester (Innovatest Europe bv, Maastricht, The Netherlands) by the Vickers method using a diamond indenter loaded at 9.81 N. Five indents were made in three different areas of the polished surface. The friction–wear properties of the composites and referential TiB<sub>2</sub> sinter sample of 97% relative density were tested in the dry sliding test in a ball-on-disc geometry (Figure 1), according to the ASTM G99-95a standard (reapproved in 2000) [11]. As a counterpart material, WC (6 wt % Co) was used. Balls 3.175 mm in diameter were loaded at 5 N. The sliding velocity was 0.1 m/s, while the total sliding distance was 200 m. The test duration was 2000 s, and the diameter of the wear track was 10 mm. Friction–wear tests were conducted in air at a relative humidity of 40–45% at room-temperature conditions. The friction force  $F_t$  was measured continuously during the test using an extensometer. For each test, a new WC ball was used. Before each test, both the ball and the sample were washed in high-purity acetone, dried in air and weighted. After mounting in the holder, the ball and the sample were washed again (in ethanol) then dried. The coefficient of friction (CoF) were calculated according to Equation (1):

$$\text{CoF} = F_t / F_n \quad (1)$$

where  $F_t$  is the measured friction force (N), and  $F_n$  is the load applied (N).

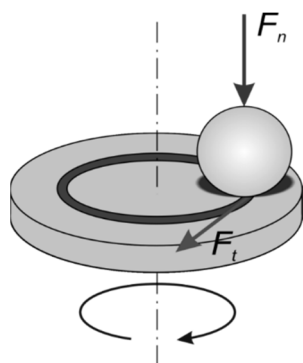


**Figure 1.** Ball-on-disc geometry of the friction–wear test.

The specific wear rate of the specimens (disc and ball) was calculated from the mass difference of each specimen before and after the ball-on-disc tests, according to Equation (2):

$$W_v = \frac{m_a - m_b}{F_n \times d \times L} \quad (2)$$

where  $W_v$  is the specific wear rate ( $\text{mm}^3/\text{Nm}$ ),  $m_a$  is the mass before the test (kg),  $m_b$  is the mass after the test (kg),  $F_n$  is the applied load (N) and  $d$  is the theoretical density ( $\text{kg}/\text{m}^3$ ).

The microstructure of the composites was observed using SEM before and after the friction–wear test. Microstructure observations were accompanied by EDS analysis.

### 3. Results

#### 3.1. SPS Sintering

The variation of temperature, applied force (pressure), punch displacement (piston movement) and sintering speed during the SPS cycle is shown in Figure 2. The observed changes in the piston displacement determine the five stages of changes that take place during sintering (I–VI) to represent the accompanying phenomena. In Stage I, particle rearrangement takes place initiated by the applied force. A positive punch displacement is recorded (Stages I and III). In between (Stage II), degassing of the powder mixture under constant temperature and force takes place. In Stage IV, a slight negative piston displacement is recorded, caused by a temperature increase from 400 °C up to the requisite sintering temperature of 1700 °C. At Stage V, the piston, after initial positive displacement,

stabilizes at a constant level. At this stage, the pores have to be eliminated. The last stage (Stage VI) is the cooling stage. Further positive piston displacement is observed due to thermally induced contraction.

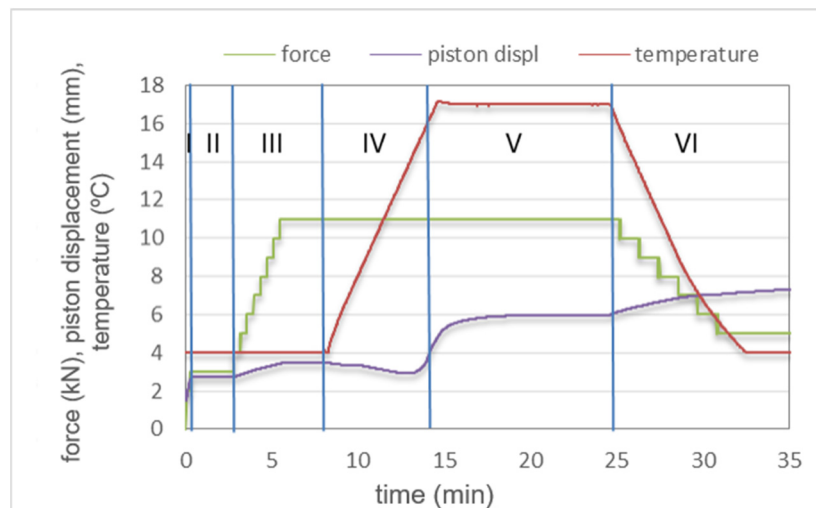


**Figure 2.** Experimental plot showing changes in applied force, piston displacement and temperature during the SPS sintering of the  $\text{TiB}_2/20 \text{ wt } \% \text{Ti}_5\text{Si}_3$  powders ( $t_{\text{max}} 1700 \text{ }^\circ\text{C}/10 \text{ min}$ ).

### 3.2. Relative Density

The powder mixture composition, sintering parameters and relative density values of the obtained materials are shown in Table 1 and compared to the  $\text{TiB}_2$  sinter produced by SPS at  $1700 \text{ }^\circ\text{C}$ . The relative density of the  $\text{TiB}_2$  sinter is low in comparison to those in References [4,12]. This sinter was produced using the same  $\text{TiB}_2$  powder and in the same sintering conditions as the composites and was used as the referential sample. In general, the relative density of the  $\text{TiB}_2/\text{Ti}_5\text{Si}_3$  composites is increased in comparison to the relative density of the  $\text{TiB}_2$  sinter and increases with the sintering temperature and titanium silicide content. This enhanced density of the produced composites comes at the expense of their hardness. As the applied temperatures of sintering are lower than the melting point of  $\text{Ti}_5\text{Si}_3$ , the process does not involve a liquid phase, as is the case of composites with the addition of  $\text{TiSi}_2$  sintered at temperatures above  $1500 \text{ }^\circ\text{C}$ ; therefore, such high densities are not obtained. However, our composites can operate at temperatures higher than  $1500 \text{ }^\circ\text{C}$ .

**Table 1.** Initial phase composition of the powder mixtures and phase composition of the samples after SPS sintering, their hardness and relative density.

Powder Mixture Composition	SPS Conditions Temperature/Time	Phase Composition after Sintering	$\rho$ Theoretical (%)	Hardness
$\text{TiB}_2/10 \text{ wt } \% \text{Ti}_5\text{Si}_3$	$1600 \text{ }^\circ\text{C}/35 \text{ MPa}/10 \text{ min}$	$\text{TiB}_2/7 \text{ wt } \% \text{Ti}_5\text{Si}_3/3 \text{ wt } \% \text{TiC}$	94.8	$1961 \pm 15 \text{ HV1}$
$\text{TiB}_2/10 \text{ wt } \% \text{Ti}_5\text{Si}_3$	$1700 \text{ }^\circ\text{C}/35 \text{ MPa}/10 \text{ min}$	$\text{TiB}_2/8 \text{ wt } \% \text{Ti}_5\text{Si}_3/4 \text{ wt } \% \text{TiC}$	96.5	$2180 \pm 28 \text{ HV1}$
$\text{TiB}_2/20 \text{ wt } \% \text{Ti}_5\text{Si}_3$	$1600 \text{ }^\circ\text{C}/35 \text{ MPa}/10 \text{ min}$	$\text{TiB}_2/16 \text{ wt } \% \text{Ti}_5\text{Si}_3/2 \text{ wt } \% \text{TiC}$	96.9	$1864 \pm 40 \text{ HV1}$
$\text{TiB}_2/20 \text{ wt } \% \text{Ti}_5\text{Si}_3$	$1700 \text{ }^\circ\text{C}/35 \text{ MPa}/10 \text{ min}$	$\text{TiB}_2/16 \text{ wt } \% \text{Ti}_5\text{Si}_3/2 \text{ wt } \% \text{TiC}$	98.2	$1953 \pm 34 \text{ HV1}$
$\text{TiB}_2$	$1700 \text{ }^\circ\text{C}/35 \text{ MPa}/10 \text{ min}$	$\text{TiB}_2$	78.6	$2400 \pm 45 \text{ HV1}$

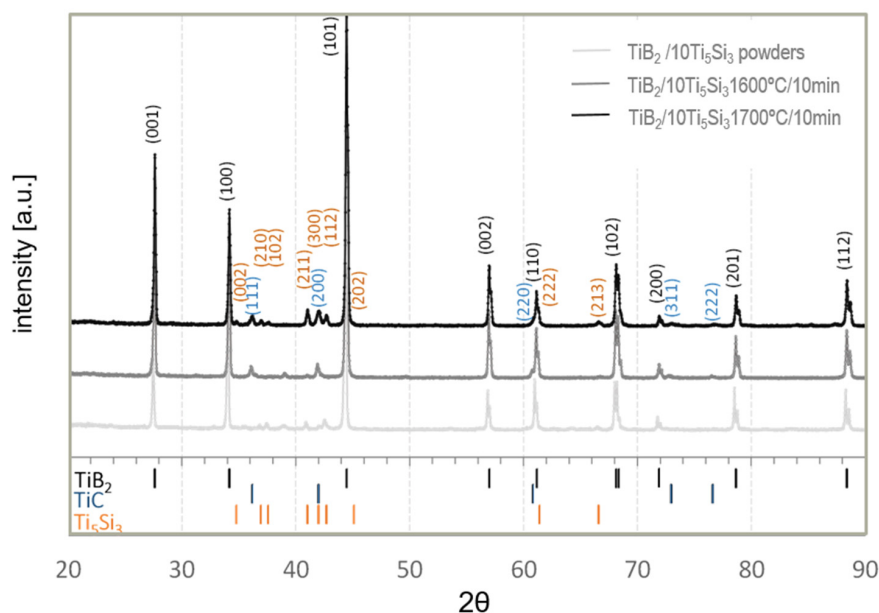
### 3.3. Microstructure

Figure 3 shows the X-ray diffraction spectra registered for the  $\text{TiB}_2/10 \text{ Ti}_5\text{Si}_3$  powder mixture after three-step homogenization and the  $\text{TiB}_2/10 \text{ wt } \% \text{Ti}_5\text{Si}_3$  composites. The XRD analysis results confirm that the major phase present in the powder mixture after homogenization and in the produced composites is  $\text{TiB}_2$  (hexagonal closest packed (hcp)).

The second phase identified in both powder mixtures and the  $\text{TiB}_2/10 \text{ Ti}_5\text{Si}_3$  and  $\text{TiB}_2/20 \text{ Ti}_5\text{Si}_3$  composites was  $\text{Ti}_5\text{Si}_3$  (D88 crystal structure of the  $\text{Mn}_5\text{Si}_3$ ). The lattice constants for this silicide identified in the powder sample were  $a = 7.465 \text{ \AA}$  and  $c = 5.168 \text{ \AA}$ ,

while in the composites,  $a = 7.4224\text{--}7.4494 \text{ \AA}$  and  $c = 5.1501\text{--}5.1506 \text{ \AA}$  were slightly reduced, probably as a result of the applied pressure during sintering. The presence of boron or carbon solid solutions in this silicide that could be formed (Nowotny phase) [13] was not found, and changes in the size of the unit cell parameters did not indicate this.

Traces of the TiC phase were detected in the composites as a result of the chemical reaction of titanium from the powder mixture and carbon from the graphite components of the sintering die. The TiC content was 2–4 wt % of the produced composites. Although a higher sintering temperature favors an increase in the diffusion rate, no significant differences were observed in the amount of this carbide in our composites. Because the titanium silicide content calculated in the composites is lower than assumed in the initial powder mixtures, with almost the preserved amount of titanium diboride, the formation of titanium carbide probably takes place at the expense of the loss of the titanium silicide. However, other phases forming the Ti-Si or Ti-Si-B system were not identified, which may be due to the evaporation of Si ( $T_m = 1414 \text{ }^\circ\text{C}$ ) or the low content of these phases in the produced composites, below XRD's detectability.



**Figure 3.** XRD patterns, registered in BB geometry of the  $\text{TiB}_2 + 10 \text{ wt } \% \text{ Ti}_5\text{Si}_3$  powder mixture after homogenization, and the  $\text{TiB}_2/10\text{Ti}_5\text{Si}_3$  composites (1600 °C and 1700 °C) with indexed peak positions for the identified phases. ICDD (ref. code) used for the identification of  $\text{TiB}_2$  (01-075-1045),  $\text{Ti}_5\text{Si}_3$  (01-078-1429) and TiC (03-065-8805).

SEM observations of the microstructure of the produced composites indicate the presence of two kinds of grains, different in chemical composition (Figures 4 and 5). Figure 4 shows a general SEM image of the microstructure of the composites  $\text{TiB}_2/10 \text{ Ti}_5\text{Si}_3$  (Figure 4a) and  $\text{TiB}_2/20 \text{ Ti}_5\text{Si}_3$  (Figure 4b) with EDS maps of the elemental distribution of Ti, B and Si. Areas clearly enriched in Si are unevenly dispersed in a homogeneous matrix in terms of the content of B and Ti (Figure 4, EDS maps). The surface of Si-enriched areas increases with the addition of titanium silicide. Some grain growth is observed with sintering temperature. In the SEM images of the microstructure of composites produced with a higher titanium silicide content, Si-rich areas are larger and easily recognizable as light-gray components of the microstructure of an irregular shape distributed in the dark-gray matrix. The darkest areas are pores. Figure 5a shows an SEM image showing the microstructure of  $\text{TiB}_2/10 \text{ Ti}_5\text{Si}_3$  with marked areas for EDS analysis and EDS spectra taken from them (Figure 5b–d). In this magnified image, some pores are evident. They most often occur within the grain boundaries, often in the vicinity of grains rich in Si, which may be a result of the evaporation of this element as the sintering temperature was  $\sim 150\text{--}250 \text{ }^\circ\text{C}$

above its melting point. Silicon evaporation may be the reason for the failure in achieving the full density of our composites. The loss of this element may cause differences in the Ti/Si ratio in the selected areas of the produced composites, as shown in Figure 5 (EDS Spectra 1 and 3)

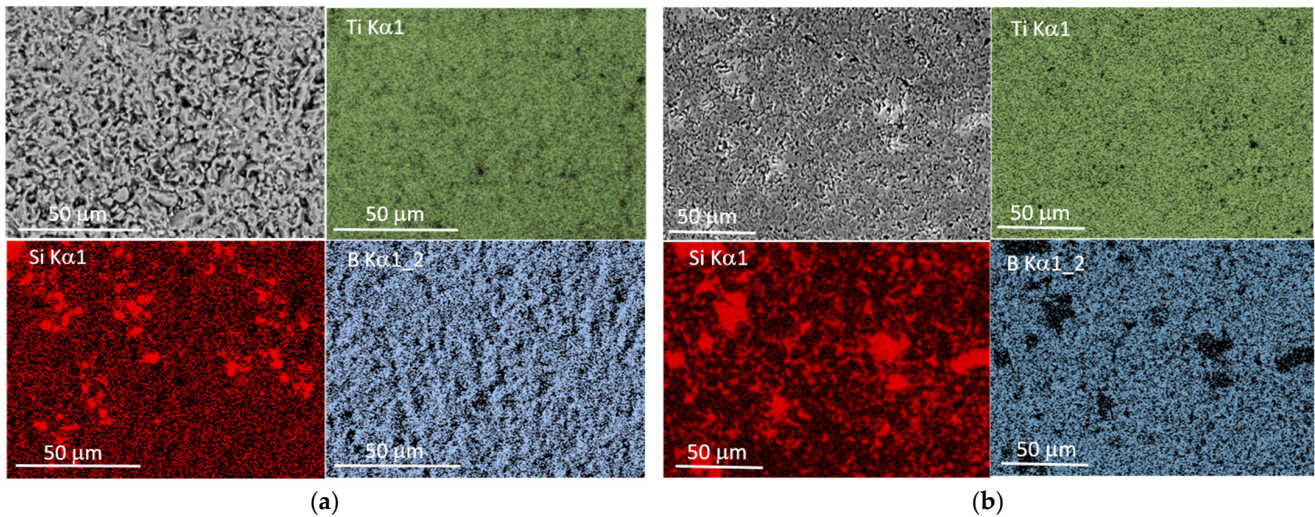


**Figure 4.** SEM images of the microstructure of the  $\text{TiB}_2/10\text{Ti}_5\text{Si}_3$  (a) and  $\text{TiB}_2/20\text{Ti}_5\text{Si}_3$  (b) composites produced by the SPS method (general view with EDS maps showing the Si, B and Ti distribution).

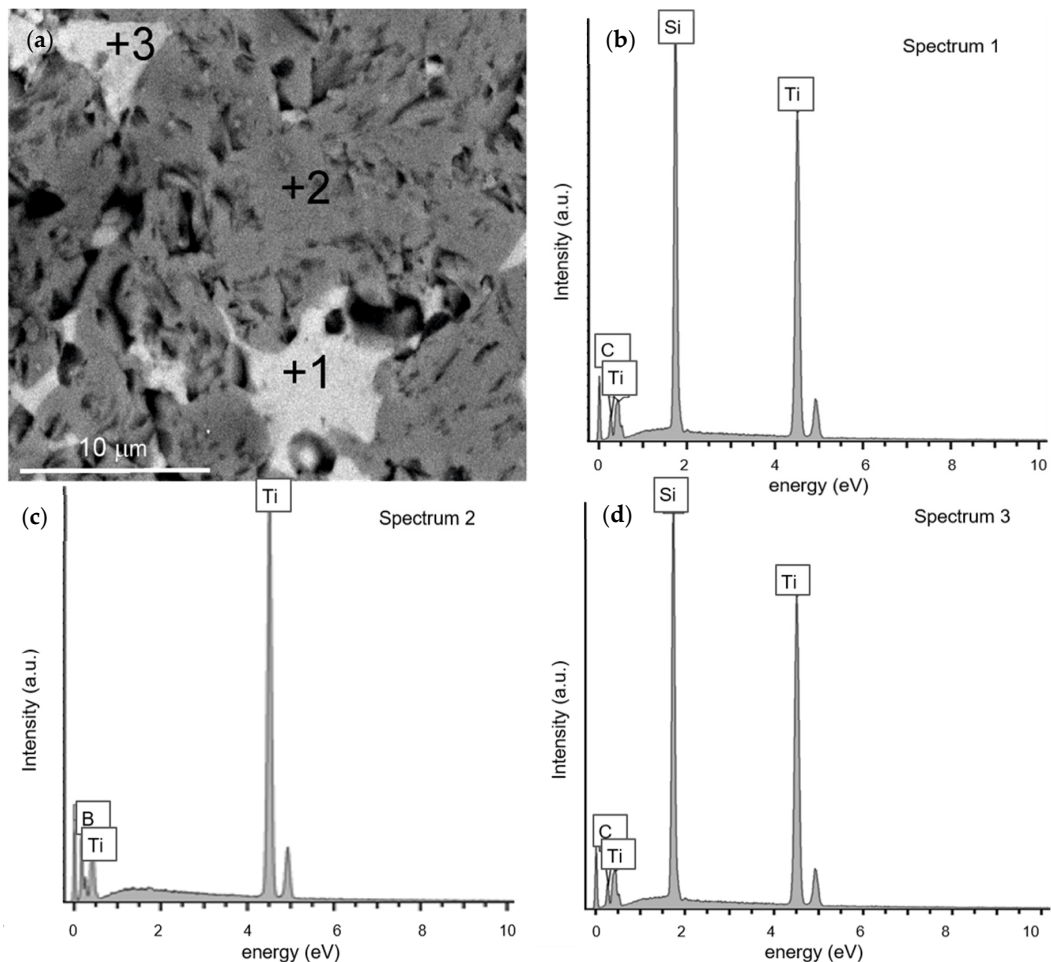


**Figure 5.** (a) SEM image of the microstructure of the  $\text{TiB}_2/10\text{Ti}_5\text{Si}_3$  composite (1600 °C/10 min) with marked areas for EDS analysis; (b–d) EDS spectra taken from them.

### 3.4. Hardness and Friction–Wear Properties

The average hardness values of the produced  $\text{TiB}_2/\text{Ti}_5\text{Si}_3$  composites are given in Table 1 and compared to the hardness measured for the  $\text{TiB}_2$  sinter produced by SPS at  $1700\text{ }^\circ\text{C}/10\text{ min}$ . SPS sintering of  $\text{TiB}_2$  powders at  $1600\text{ }^\circ\text{C}$  was not effective, and the material densified at the lower sintering temperature was not qualified for further research.

Detailed SEM observation of the surfaces of the  $\text{TiB}_2/\text{Ti}_5\text{Si}_3$  composites after the hardness test (Figure 6a,b) indicated that the produced materials were brittle. In the indented area and in its close proximity, there were splinters and/or chippings. Cracking in the corners of the produced indents was evident and propagated intergranular. The susceptibility to chipping and radial cracking formation was increased in the composites containing 20 wt % of titanium silicide addition in comparison to those containing 10 wt % of silicide addition. Strong chipping of the surface under the indenter made the hardness measurement difficult or even impossible. The presence of chipping and spallation of the surface of the specimens near the imprints made it impossible to calculate  $K_{\text{IC}}$ . In general, there are no data that can be found in the field of the microstructure and properties of  $\text{TiB}_2$  composites prepared by the SPS method with  $\text{Ti}_5\text{Si}_3$  as a sintering aid; however, this phase is often identified in composites produced by the sintering of  $\text{TiB}_2$  powder with  $\text{TiSi}_2$  [9,14] or  $\text{MoSi}_2$  [15] sintering additives. The  $\text{Ti}_5\text{Si}_3$  phase occurs in these composites as an unwanted product of the reactions between  $\text{TiB}_2$  and  $\text{TiSi}_2$ , occurring during spark plasma sintering at  $1400\text{--}1650\text{ }^\circ\text{C}$  for 10 min but also in composites sintered at a relatively low temperature of  $1200\text{ }^\circ\text{C}$  but for a longer time duration (i.e., 30 min). In a material containing 5 wt %  $\text{TiSi}_2$ , the  $\text{Ti}_5\text{Si}_3$  phase was observed near the interfaces in between the  $\text{TiB}_2$  and  $\text{TiSi}_2$  grains as a layer of 50–100 nm in thickness. Unfortunately, despite the fact that this phase was identified by XRD, its content was not estimated, so its influence on the mechanical properties of produced material is not known. In the absence of information, it remains to compare the measured hardness values to the calculated values on the basis of the rule of mixtures. Assuming  $\text{TiB}_2$  hardness of 2400 HV1 (Table 1) and  $\text{Ti}_5\text{Si}_3$  hardness of 986 HV1, according to [16], the calculated hardness values are  $\sim 2258\text{ HV1}$  for  $\text{TiB}_2/10\text{ wt } \%$   $\text{Ti}_5\text{Si}_3$  composites and  $2117\text{ HV1}$ -for  $\text{TiB}_2/20\text{ wt } \%$   $\text{Ti}_5\text{Si}_3$ , which correspond to the measured values (Table 1). The decrease in the hardness of the produced composites with  $\text{Ti}_5\text{Si}_3$  content is not surprising, as similar degradation of the properties of the  $\text{TiB}_2$ -based composites is observed with the addition of other phases beyond 5 wt % of similar hardness to that of  $\text{TiB}_2$ , such as  $\text{MoSi}_2$  [15].

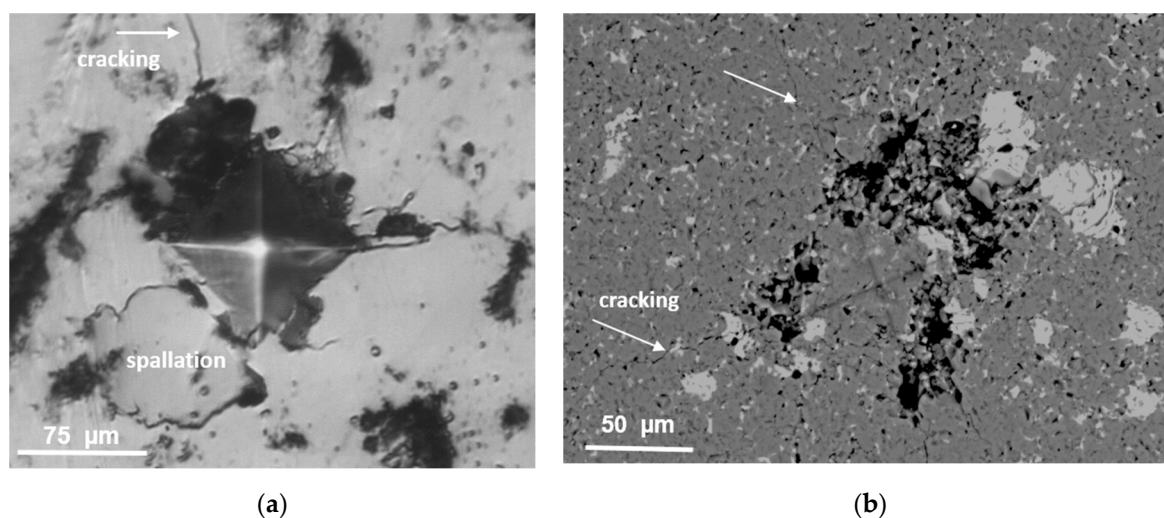


**Figure 6.** (a) Light microscopy image of the surface of the indented area:  $\text{TiB}_2/10\text{ Ti}_5\text{Si}_3$  composite sintered at  $1600\text{ }^\circ\text{C}$  (b); SEM image of the surface of the indented area of the  $\text{TiB}_2/20\text{ Ti}_5\text{Si}_3$  composite sintered at  $1600\text{ }^\circ\text{C}$ .

The friction–wear properties of the  $\text{TiB}_2/\text{Ti}_5\text{Si}_3$  composites were examined in the ball-on-disc test without the use of lubricants. In our experiments, the resistance to wear of

the tested samples was determined against a WC ball, as was already been applied in our previous studies for  $\text{TiB}_2$  sinters [17]. Figure 7 shows the CoF and wear rate plots of the composite samples tested in the dry sliding test (ball-on-disc test). The addition of  $\text{Ti}_5\text{Si}_3$  significantly reduces the wear rate of the produced composites. With an increased content of  $\text{Ti}_5\text{Si}_3$ , a decrease in the coefficient of friction values is noted at a low number of cycles ( $N < 2000$ ) but does not influence the average value of the COF, as shown in Figure 8.

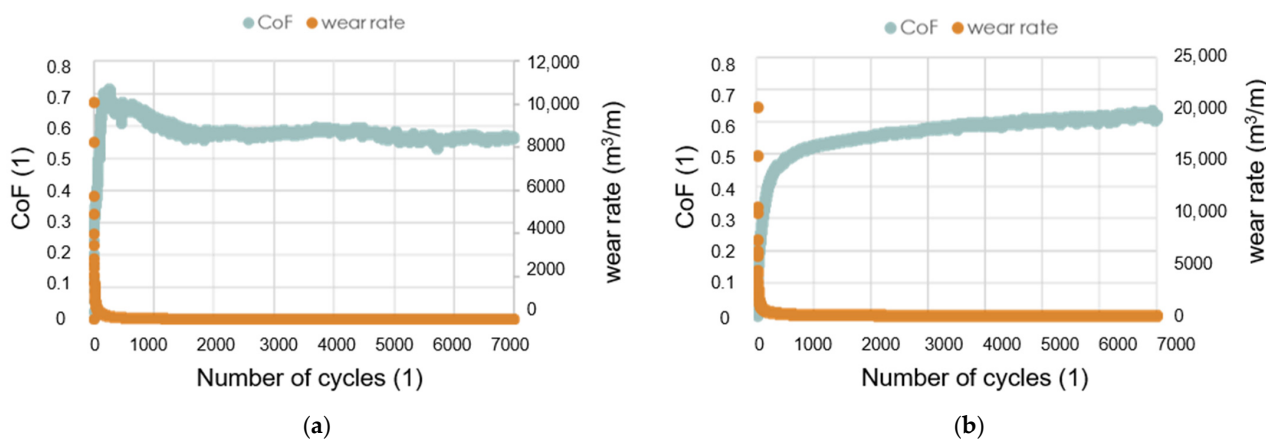


**Figure 7.** Experimental plots of the CoF and the wear rate of the SPS sinters tested in the dry sliding test with WC as a counterpart: (a)  $\text{TiB}_2/10\text{Ti}_5\text{Si}_3$  1600 °C; (b)  $\text{TiB}_2/20\text{Ti}_5\text{Si}_3$  1700 °C.

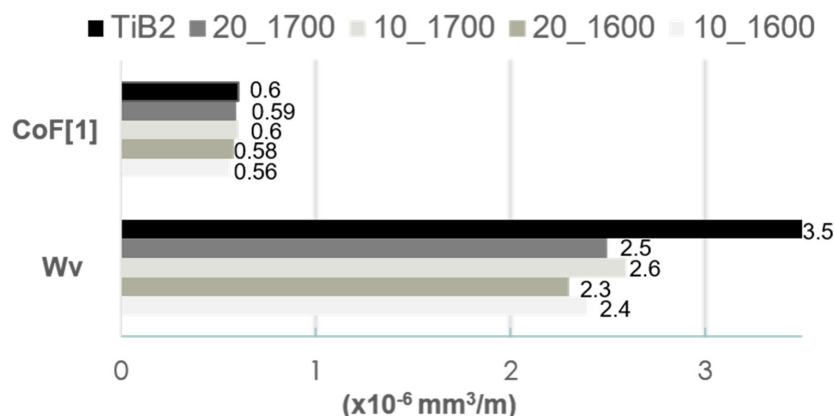


**Figure 8.** CoF values and volumetric wear indexes ( $W_v$ ) of the  $\text{TiB}_2/\text{Ti}_5\text{Si}_3$  composites determined in friction contact with WC balls loaded at 5 N.

The specific wear rate values  $W_v$  are relatively low and similar for all produced composites. In comparison to the value for the referential  $\text{TiB}_2$  sinter tested with the WC ball in the same ball-on-disc test parameters, it was reduced by ~28 %. To understand the cause of the significant increase in the wear resistance with  $\text{Ti}_5\text{Si}_3$  content, the wear tracks were subjected to detailed microstructural observations with the use of a scanning electron microscope (Figure 9) and accompanying analyses of the chemical composition by the EDS method.

In the areas of the friction track, numerous grooves were observed, which are typical signs of abrasive wear. EDS maps registered from worn areas indicated the presence of oxygen in the worn area, as well as traces of tungsten and carbon. The presence of boron oxides (and hydroxides), as well as titanium and silicon oxides, was the result of the tribo-oxidation of Ti, B and Si coming from the tested composite samples. Traces of W and C, which were also detected by EDS, come from the WC ball. The distribution of W (Figure 10) also indicates the presence of the tribo-oxidation products of this element. Tungsten and titanium suboxides belong to the group of Magnéli phases with lubricating



properties [18,19]. Hydrogenated boron oxides have similar lubricating properties. Their presence in the friction contact area is favorable; however, they do not significantly affect the CoF value (Figure 8). Clearly, tribo-oxidation takes place at the expense of the weight loss of both materials in frictional contact, but the formation of oxides compensates for this loss, which, in turn, has a positive effect on the specific wear rate values.

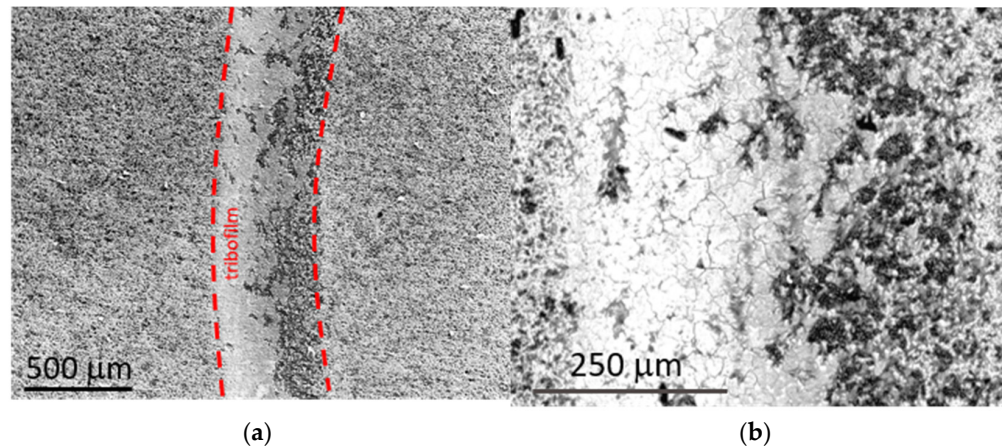


**Figure 9.** SEM images of the surface of the  $\text{TiB}_2/20 \text{ wt } \% \text{ Ti}_5\text{Si}_3$  composite after the ball-on disc test: (a) general view (low-vacuum SE image); (b) magnified SEM image of the wear track area.

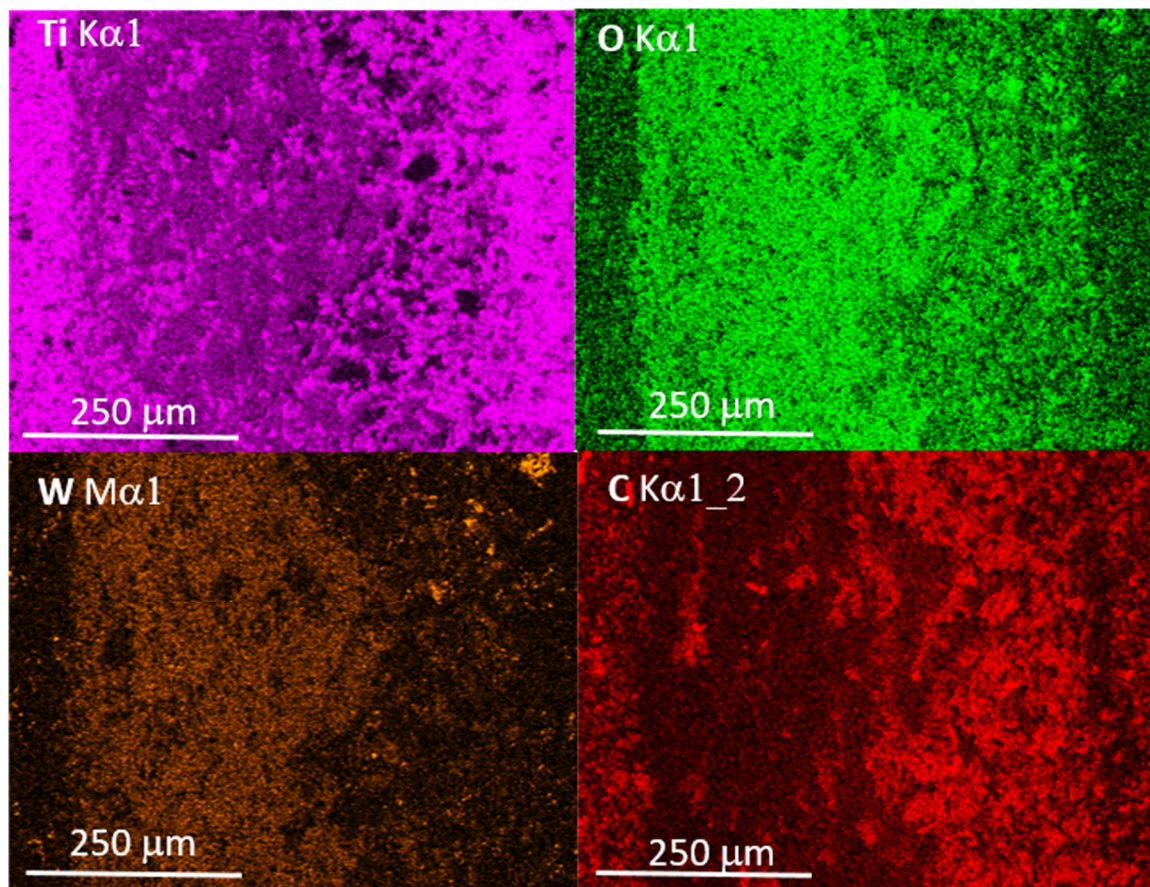


**Figure 10.** EDS elemental maps of Ti, O, W and C registered from the area presented in Figure 9b.

#### 4. Conclusions

The effects of sintering temperature and  $\text{Ti}_5\text{Si}_3$  content on the microstructure of  $\text{TiB}_2/\text{Ti}_5\text{Si}_3$  composites, their density, hardness and friction–wear properties were investigated and discussed. Based on the experimental results and analysis, the following major conclusions were reached:

- Spark plasma sintering is an effective and fast method for the densification of  $\text{TiB}_2/\text{Ti}_5\text{Si}_3$  powders. The addition of 10–20 wt % of  $\text{Ti}_5\text{Si}_3$  is beneficial for the density of  $\text{TiB}_2/\text{Ti}_5\text{Si}_3$  composites. The relative density of the produced composites is up to 98.4% of the theoretical composites.
- SPS sintering of the  $\text{TiB}_2/\text{Ti}_5\text{Si}_3$  initial powders at 1600 °C and 1700 °C results in the formation of TiC due to the effect of carbon diffusion from the graphite components of the sintering die.
- The hardness of the produced composites decreases with  $\text{Ti}_5\text{Si}_3$  content, but their resistance to wear in friction contact with WC increases with it, and for composites containing 20% of this additive, it increases by almost 30%.
- The main mechanism of wear is abrasion. The presence of titanium, tungsten and boron oxides at worn areas indicate the tribo-oxidation reactions of these elements.
- The COF values of  $\text{TiB}_2/\text{Ti}_5\text{Si}_3$  composites in friction contact with WC were in the range of 0.54–0.61, similar to the value of the  $\text{TiB}_2$  sinter.

**Author Contributions:** Conceptualization, A.T.; methodology, A.T. and M.P.; validation, K.B., P.H. and I.S.; formal analysis, A.T.; investigation, I.S. and P.H.; resources, A.T.; data curation, K.B. writing—original draft preparation, A.T.; writing—review and editing, A.T.; project administration, A.T.; funding acquisition, A.T. All authors have read and agreed to the published version of the manuscript.

**Funding:** This research received no external funding.

**Institutional Review Board Statement:** Not applicable.

**Informed Consent Statement:** Not applicable.

**Data Availability Statement:** The data presented in this study are available on request from the corresponding author.

**Acknowledgments:** This work was financially supported by Pedagogical University in Krakow, Poland, within the research project WPBU/2020/05/00195.

**Conflicts of Interest:** The authors declare no conflict of interest.

#### References

1. Munro, R.G. Material Properties of Titanium Diboride. *J. Res. Natl. Inst. Stand. Technol.* **2000**, *105*, 709–720. [[CrossRef](#)] [[PubMed](#)]
2. Basu, B.; Raju, G.B.; Suri, A.K. Processing and properties of monolithic  $\text{TiB}_2$ -based materials. *Int. Mater. Rev.* **2006**, *51*, 352–374. [[CrossRef](#)]
3. Twardowska, A.; Morgiel, J.; Rajchel, B. Thermally Induced Crystallization of  $\text{TiB}_x$  Thin Film after Deposition by Dual Beam IBAD Method. *Mater. Today Proc.* **2016**, *3*, 2646–2651. [[CrossRef](#)]
4. Balci, Ö.; Burkhardt, U.; Schmidt, M.; Hennicke, J.; Yagci, M.B.; Somer, M. Densification, microstructure and properties of  $\text{TiB}_2$  ceramics fabricated by spark plasma sintering. *Mater. Charact.* **2018**, *145*, 435–443. [[CrossRef](#)]
5. Park, J.-H.; Koh, Y.-H.; Kim, H.-E.; Hwang, C.S.; Kang, E.S. Densification and Mechanical Properties of Titanium Diboride with Silicon Nitride as a Sintering Aid. *J. Am. Ceram. Soc.* **2004**, *82*, 3037–3042. [[CrossRef](#)]
6. Vallauri, D.; Adrian, I.A.; Chrysanthou, A.  $\text{TiC-TiB}_2$  composites: A review of phase relationships, processing and properties. *J. Eur. Ceram. Soc.* **2008**, *28*, 1697–1713. [[CrossRef](#)]
7. Murthy, T.S.R.C.; Basu, B.; Balasubramaniam, R.; Suri, A.K.; Subramanian, C.; Fotedar, R.K. Processing and Properties of  $\text{TiB}_2$  with  $\text{MoSi}_2$  Sinter-additive: A First Report. *J. Am. Ceram. Soc.* **2005**, *89*, 131–138. [[CrossRef](#)]
8. Murthy, T.S.R.C.; Subramanian, C.; Fotedar, R.; Gonal, M.; Sengupta, P.; Kumar, S.; Suri, A. Preparation and property evaluation of  $\text{TiB}_2+\text{TiSi}_2$  composite. *Int. J. Refract. Met. Hard Mater.* **2009**, *27*, 629–636. [[CrossRef](#)]
9. Raju, G.B.; Basu, B. Densification, sintering reactions, and properties of titanium diboride with titanium disilicide as a sintering aid. *J. Am. Ceram. Soc.* **2007**, *90*, 3415–3423. [[CrossRef](#)]
10. Mitra, R. Mechanical behavior and oxidation resistance of structural silicides. *Int. Mater. Rev.* **2006**, *51*, 13–64. [[CrossRef](#)]

11. ASTM G99-17. *Standard Test Method for Wear Testing with a Pin-on-Disk Apparatus*; ASTM International: West Conshohocken, PA, USA, 2017.
12. Demirskyi, D.; Sakka, Y. High-temperature reaction consolidation of TaC–TiB<sub>2</sub> ceramic composites by spark-plasma sintering. *J. Eur. Ceram. Soc.* **2015**, *35*, 405–410. [[CrossRef](#)]
13. Wdowik, U.D.; Wasik, M.; Twardowska, A. Influence of carbon dopants on the structure, elasticity and lattice dynamics of Ti<sub>5</sub>Si<sub>3</sub>C<sub>x</sub>Nowotny phases. *Model. Simul. Mater. Sci. Eng.* **2016**, *24*, 025001. [[CrossRef](#)]
14. Jain, D.; Reddy, K.M.; Mukhopadhyay, A.; Basu, B. Achieving uniform microstructure and superior mechanical properties in ultrafine grained TiB<sub>2</sub>–TiSi<sub>2</sub> composites using innovative multi stage spark plasma sintering. *Mater. Sci. Eng. A* **2010**, *528*, 200–207. [[CrossRef](#)]
15. Mukhopadhyay, A.; Raju, G.; Basu, B.; Suri, A. Correlation between phase evolution, mechanical properties and instrumented indentation response of TiB<sub>2</sub>-based ceramics. *J. Eur. Ceram. Soc.* **2009**, *29*, 505–516. [[CrossRef](#)]
16. Rosenkranz, R.; Frommeyer, G.; Smarsly, W. Microstructures and properties of high melting point intermetallic Ti<sub>5</sub>Si<sub>3</sub> and TiSi<sub>2</sub> compounds. *Mater. Sci. Eng. A* **1992**, *152*, 288–294. [[CrossRef](#)]
17. Sulima, I.; Figiel, P.; Suśniak, M.; Świątek, M. Sintering of TiB<sub>2</sub> ceramics. *Arch. Mater. Sci. Eng.* **2007**, *28*, 687–690.
18. Scharf, T.W.; Rajendran, A.; Banerjee, R.; Sequeda, F. Growth, structure and friction behavior of titanium doped tungsten disulphide (Ti-WS<sub>2</sub>) nanocomposite thin films. *Thin Solid Film.* **2009**, *517*, 5666–5675. [[CrossRef](#)]
19. Woydt, M. Tribological characteristics of polycrystalline Magnéli-type titanium dioxides. *Tribol. Lett.* **2000**, *8*, 117–130. [[CrossRef](#)]